

## RESEARCH ARTICLE

10.1002/2014JG002710

## Key Points:

- NPP/RUE profiles show nonlinear behaviors across a precipitation gradient
- Interannual NPP variability is related to monsoon precipitation climatology
- Long-term positive trends in RUE may reveal ecosystem acclimation

## Supporting Information:

- Readme
- Table S1
- Figure S1
- Figure S2
- Figure S3
- Figure S4

## Correspondence to:

G. Forzieri,  
[giovanni.forzieri@jrc.ec.europa.eu](mailto:giovanni.forzieri@jrc.ec.europa.eu)

## Citation:

Forzieri, G., L. Feyen, A. Cescatti, and E. R. Vivoni (2014), Spatial and temporal variations in ecosystem response to monsoon precipitation variability in southwestern North America, *J. Geophys. Res. Biogeosci.*, 119, 1999–2017, doi:10.1002/2014JG002710.

Received 14 MAY 2014

Accepted 13 SEP 2014

Accepted article online 18 SEP 2014

Published online 28 OCT 2014

This is an open access article under the terms of the Creative Commons Attribution-NonCommercial-NoDerivs License, which permits use and distribution in any medium, provided the original work is properly cited, the use is non-commercial and no modifications or adaptations are made.

# Spatial and temporal variations in ecosystem response to monsoon precipitation variability in southwestern North America

Giovanni Forzieri<sup>1</sup>, Luc Feyen<sup>1</sup>, Alessandro Cescatti<sup>1</sup>, and Enrique R. Vivoni<sup>2</sup>
<sup>1</sup>European Commission, Joint Research Centre (JRC), Institute for Environment and Sustainability (IES), Climate Risk Management Unit, Ispra, Italy, <sup>2</sup>School of Earth and Space Exploration and School of Sustainable Engineering and the Built Environment, Arizona State University, Tempe, Arizona, USA

**Abstract** Due to its marked vegetation phenology and precipitation gradients, the North American Monsoon Region (NAMR) is a useful domain for studying ecosystem responses to climate variability and change. To this end, we analyze long-term dynamics (1982–2004) in monsoon precipitation (Pr), time-integrated Normalized Difference Vegetation Index (TINDVI) used as proxy of net primary productivity, and rain-use efficiency (RUE). The analysis focuses on six ecoregions, spanning from desert environments to tropical dry forests, to investigate (1) how net primary productivity and rain-use efficiency vary along a precipitation gradient, (2) if interannual variability in net primary productivity is linked to the interannual variability in precipitation, and (3) if there is evidence of a long-term signal imposed on the interannual variability in rain-use efficiency. Variations in TINDVI and RUE with Pr along the NAMR precipitation gradient differ among ecoregions exhibiting intensive or extensive water use strategies. We explain the nonlinear behaviors along the precipitation gradient as resulting from different physiological responses to climatological means and the impact of topographic effects. Statistical analysis indicates that the interannual variability in vegetation response is significantly related to the interannual variability in Pr, but their correlation declines with time. A long-term positive signal in RUE imposed on its interannual variability is identified and results from a constant TINDVI under negative long-term trends of Pr. This important finding suggests the combined long-term effects of ecosystem acclimation to reduced water availability and increasing CO<sub>2</sub> concentration across the varied ecosystems of the North American Monsoon Region.

## 1. Introduction

Spatial and temporal patterns of water availability are essential drivers of biological processes in over 40% of terrestrial biomes [Nemani *et al.*, 2003]. Precipitation is the primary input of this limiting resource and controls both biotic and abiotic processes through soil moisture redistribution [e.g., Noy-Meir, 1973; Webb *et al.*, 1986; Rodríguez-Iturbe, 2000; Weltzin *et al.*, 2003; Méndez-Barroso *et al.*, 2009]. Seasonal precipitations explain much of the variability of ecosystem primary productivity and are important drivers of ecosystem functioning [Knapp and Smith, 2001; Huxman *et al.*, 2004]. This is particularly evident in southwestern North America, where the North American monsoon accounts for about 50–80% of the annual precipitation during July–September [Higgins *et al.*, 1997; Sheppard *et al.*, 2002; Vivoni *et al.*, 2008]. Exploring the ecosystem responses to rainfall variability within the North American Monsoon Region (NAMR) is of particular interest given the range of diverse ecosystems, spanning from deserts to tropical deciduous forests, which are organized along a precipitation gradient [e.g., Brown, 1994; Salinas-Zavala *et al.*, 2002; Vivoni, 2012; Forzieri *et al.*, 2011, 2013].

The assessment of ecosystem efficiency in exploiting available water for primary production is a key to understanding vegetation-climate interactions and for predicting ecosystem responses to global change. This is relevant in view of the projections of changing precipitation regimes across southwest U.S. and northwest Mexico under climate change [e.g., Seager *et al.*, 2007; Kirtman *et al.*, 2013; Mearns *et al.*, 2013; Maloney *et al.*, 2014]. Recent studies project negligible changes in total monsoon season rainfall with greenhouse gas warming, but significant declines in early monsoon season precipitation (June–July) and increases in late monsoon season (September–October) precipitation by the end of the twenty-first century [Cook and Seager, 2013]. Such a shift in the seasonal distribution of precipitation could potentially drive a spatial reorganization of ecosystems with impacts on the surface water and energy balance [e.g., Weltzin *et al.*, 2003; Chapin *et al.*, 2009; Notaro *et al.*, 2012; Williams *et al.*, 2012]. However, investigating the spatial and temporal variations of ecosystem responses to

precipitation presents some limitations related to the reliability and representativeness of vegetation data for large-scale analyses [Weltzin *et al.*, 2003; Asbjornsen *et al.*, 2011]. In addition, the underlying processes linking precipitation and ecosystem productivity still require a deeper understanding for improved vegetation-atmosphere modeling [Dominguez *et al.*, 2008; Quillet *et al.*, 2010; Keenan *et al.*, 2012; Migliavacca *et al.*, 2012; Richardson *et al.*, 2012].

Net primary productivity (NPP) and rain-use efficiency (RUE)—defined as the NPP per unit precipitation—are well-known productivity indicators whose changes integrate the influence of climatological, ecological, and biogeochemical processes crucial for understanding interactions in the biosphere [e.g., Le Houérou, 1984; Prince *et al.*, 1998]. Despite efforts to develop NPP data sets from ground observations and derive consistent gridded products from these (e.g., Long Term Ecological Research, LTER, and Ecosystem Model-Data Intercomparison, EMDI, data sets), the sparse nature of these products still limits the analysis of ecosystem dynamics at regional to continental scales. Satellite-based spectral vegetation indices (VIs) have been widely used as a proxy of NPP [e.g., Reed *et al.*, 1994; White *et al.*, 1997; Prince *et al.*, 1998] or served as input into NPP retrieval algorithms [Running *et al.*, 2004; Zhao *et al.*, 2005; Eisfelder *et al.*, 2012], which are useful for deriving phenological properties at regional to global scales and over long time periods.

Quantifying NPP and RUE across a precipitation gradient may address the complex, and in some cases, contradictory picture of ecosystem responses at local sites. For example, RUE derived from ground measurements has been observed to exhibit a decreasing trend [Le Houérou, 1984; Huxman *et al.*, 2004], an increasing tendency [Bai *et al.*, 2008a], unimodal behavior [Paruelo *et al.*, 1999; O'Connor *et al.*, 2001; Yang *et al.*, 2010], or insignificant changes [Lauenroth *et al.*, 2000] with increasing precipitation. Differences in the scale of analysis and bioclimatic regimes have been claimed as the main causes of such divergences [Bai *et al.*, 2008a]. Only few remote sensing studies have quantified relations between VIs and precipitation patterns, hereby mainly focusing on NPP changes [e.g., Jobbágy *et al.*, 2002; Fang *et al.*, 2005; Méndez-Barroso *et al.*, 2009; Ivits *et al.*, 2013]. Regional-scale observational studies that analyze both NPP and RUE variations along precipitation gradients using remote sensing techniques can provide new insights of precipitation controls on vegetation greenness and be used to test theories obtained through local-scale studies or across many sites [e.g., Paruelo *et al.*, 1999; Huxman *et al.*, 2004; Bai *et al.*, 2008a; Méndez-Barroso and Vivoni, 2010].

Understanding ecosystem responses to precipitation variability is pivotal for characterizing land-atmosphere interactions. This is particularly significant in light of studies by Keenan *et al.* [2012] and Richardson *et al.* [2012], which emphasized the need for a better representation of vegetation phenology in biosphere models in order to improve the sensitivity to climate variations on interannual time scales. Prior efforts to identify relationships between interannual variations in NPP and mean annual precipitation have led to conflicting results. Some studies did not find a correlation [Goward and Prince, 1995; Knapp and Smith, 2001], while others found a positive relationship [Paruelo and Lauenroth, 1998; Fang *et al.*, 2001; Mohamed *et al.*, 2004]. There is still no clear agreement on the potential link between interannual variations in rainfall and biomass production across different ecosystems. Additional studies are therefore needed to better understand such interactions at regional scales.

Understanding vegetation responses to decadal-scale climate fluctuations is also crucial in light of global change [e.g., Cayan *et al.*, 2001; Migliavacca *et al.*, 2012; Williams *et al.*, 2012]. Several studies have analyzed long-term vegetation dynamics at regional to global scales using different modeling approaches and remote sensing products, showing over the North American Monsoon Region either decreasing [Nemani *et al.*, 2003; Zhang *et al.*, 2010] or increasing [Bai *et al.*, 2008b; Zhao and Running, 2010; Samanta *et al.*, 2011] trends in NPP in time or no changes [Forzieri *et al.*, 2011; Fensholt *et al.*, 2012]. Divergences are likely due to different temporal periods, modeling approaches, remote sensing techniques, or ecosystems studied. Beyond the conflicting results, most studies have analyzed temporal variations in NPP, while its relation with seasonal rainfall over interannual time scales has not been fully investigated. Other factors, in addition to water availability, may affect vegetation dynamics on the decadal time scale. In particular, the observed rise of about 10% in CO<sub>2</sub> concentrations over the last three decades [e.g., Hartmann *et al.*, 2013] has presumably influenced vegetation response allowing plants to photosynthesize faster, but its long-term effects are uncertain [Norby and Zak, 2011; Donohue *et al.*, 2013; Saurer *et al.*, 2014]. Exploring possible long-term dynamics in RUE—in view of both NPP and rainfall variations—could reveal important ecosystem-specific adaptation strategies to cope with changes in climate and atmospheric composition.

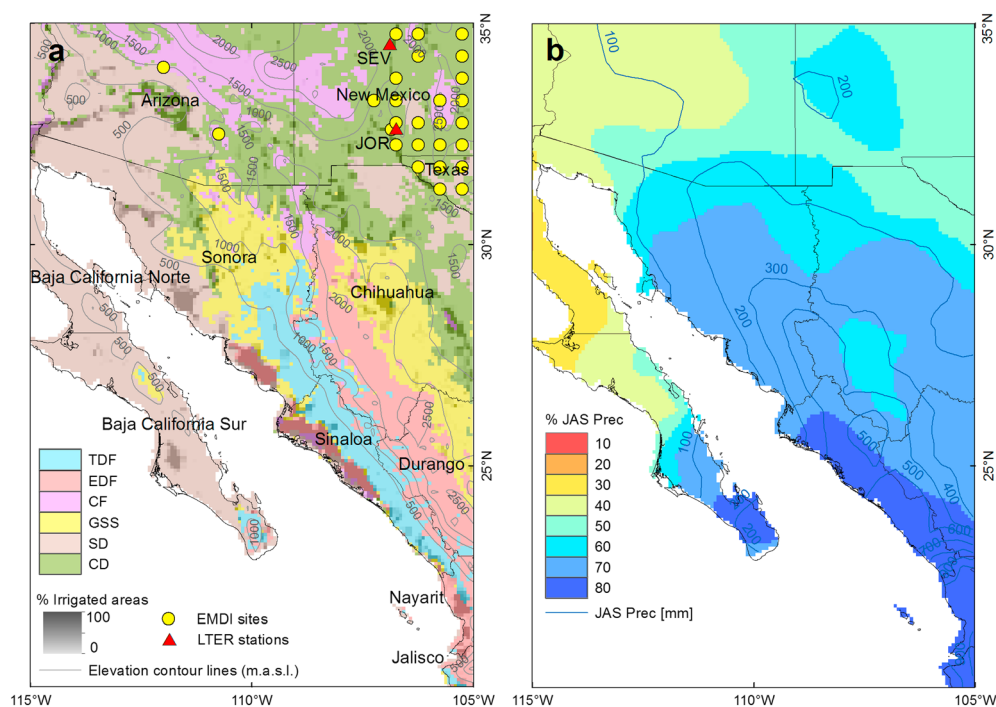


**Figure 1.** (a) North American Monsoon Region (NAMR) showing ecoregion map, LTER and EMDI sites in the domain, elevation contour lines, and percentage of irrigated area; (b) CPC-derived percentage of annual precipitation during JAS and contour lines of JAS precipitation.

The goal of this study is to quantify the interannual vegetation response to seasonal precipitation variability during the North American monsoon in six diverse ecosystems. We use long-term data sets of satellite vegetation indexes (VIs) and gridded precipitation data to address the debates concerning vegetation-climate interactions. Our work addresses the following questions: (1) How do NPP and RUE change along a precipitation gradient in the North American Monsoon Region? (2) Is the interannual variability in ecosystem responses related to the interannual fluctuations in precipitation patterns? (3) And is there evidence of a long-term climate signal imposed on the interannual variability of RUE? Understanding the relations between precipitation variability and NPP may serve to enhance the assessment of climate change impacts on vegetation dynamics.

## 2. Materials and Methods

### 2.1. Study Region and Land Surface Products

The large study region (20 to 35°N, 105 to 115°W) matches the North American Monsoon Experiment Tier I domain (Figure 1) and is referred to as the NAMR here. To characterize spatiotemporal dynamics of vegetation, we used the GIMMS (Global Inventory Modeling and Mapping Studies) 16 day composite Normalized Difference Vegetation Index (NDVI) data set, a well-known vegetation index, inferred from the AVHRR (Advanced Very High Resolution Radiometer) sensor from 1982 to 2006 at 8 km resolution [Tucker et al., 2004]. The GIMMS archive is considered one of the best data sets available for long-term NDVI trend analysis [Beck et al., 2011]. Effects related to drifting orbits and degrading sensors as well as sensor calibration, view geometry, and volcanic aerosols have been corrected to harmonize data from multiple sensors [Pinzon et al., 2005; Tucker et al., 2005] making the GIMMS product stable with respect to interannual variations [Alcaraz-Segura et al., 2010]. We applied the ecoregion map derived from Forzieri et al. [2011] to analyze the variations across different ecosystems (Figure 1a). This map was obtained through a *k*-means unsupervised classification of the three principal components of the NDVI time series. The ecoregion map shows an excellent agreement with the land cover map of the Commission for Environmental Cooperation [1997] and the classifications of Salinas-Zavala et al. [2002] and Brown [1994]. The resulting ecoregion distribution distinguishes the following: tropical dry forests (TDF) of the Pacific coastal plain, hills, and canyons;

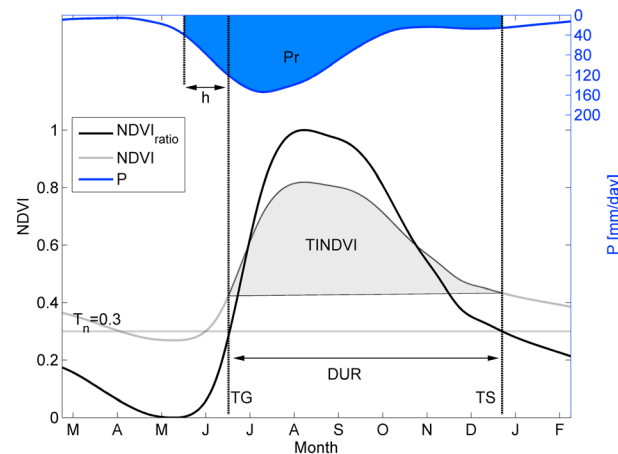


**Figure 2.** Identification of the vegetation phenological metrics based on Forzieri et al. [2011] and computation of the monsoon precipitation (Pr) based on the temporal lag (h).

Sierra Madre Occidental mountain woodlands composed of evergreen and deciduous forests (EDF); conifer forests (CF) in Arizona and New Mexico; semiarid grasslands, shrublands, and subtropical scrublands (GSS) in the Sierra Madre Occidental piedmont; Sonoran Desert (SD); and the Chihuahuan Desert (CD). We used the Global Map of Irrigation Areas, GMIA [Siebert et al., 2013], at 5 min resolution to identify areas affected by irrigation. This map was derived from statistical census data and provides the percentage of irrigated area per grid cell in 2005 (Figure 1a). We also employed a 1 km digital elevation model (DEM) from the U.S. Geological Survey HYDRO1K data set to characterize regional topography

and explore its potential role in modulating the ecosystem response to precipitation. Both the GMIA and DEM were aggregated at 8 km resolution to match the NDVI data set.

We collected annual aboveground NPP measurements from 10 LTER sites across North America with an average sampling period of 12 years over 1982–1998 [see Knapp and Smith, 2001]. The LTER sites represent a variety of terrestrial biomes which allow for the exploration of a large productivity range and include: balsam poplar forest (BNZ), oak savanna grassland (CC), mixed deciduous forest (HF and HB), black grama grassland (JOR), successional field (KG), tallgrass prairie (KNZ), moist alpine meadow (NWT), mixed desert grassland (SEV), and shortgrass steppe (SG). Of these, the JOR and SEV sites are located in the North American Monsoon Region (Figure 1a, red triangles). Furthermore, we acquired the EMDI data set [Olson et al., 2013] which was assembled from extensive worldwide NPP data collection from Oak Ridge National Laboratory Distributed Active Archive Center. The EMDI data set includes both ground NPP measurements and estimates for 0.5° grid cells for which inventory, modeling, or remote sensing tools were used to scale up the point measurements. Each individual point or gridded NPP measurement provides an annual NPP estimate calculated as an average over the overall temporal coverage 1931–1996 (the coverage does not include all years for all sites). Of the total sample of 2803 NPP measurements/estimates, 27 sites are located within the North American Monsoon Region (Figure 1a, yellow circles). As an additional validation data set, we used satellite estimates of annual terrestrial NPP derived from MODIS products (MOD17A3, Moderate Resolution Imaging Spectroradiometer) at 1 km resolution over the 2000–2006 period that partially overlaps in time with the GIMMS data set [Zhao et al., 2005]. The MOD17A3 algorithm derives NPP by combining meteorological data with the fraction of photosynthetically active radiation (fPAR) and biome-specific allometric relations. While the MODIS products represent an indirect measure of NPP, they have been validated over the global scale ( $R^2 = 0.77$  [Zhao et al., 2005]) and are therefore considered a useful comparison data set for this study. Furthermore, the MODIS product is based on spectral bands that are specifically designed for vegetation monitoring and include state-of-the-art navigation, atmospheric correction, reduced geometric distortions, and enhanced radiometric sensitivity which make MODIS data an improved product compared to AVHRR products [Huete et al., 2002].

To characterize the precipitation dynamics in the North American Monsoon Region, we used the Climate Prediction Center (CPC) daily 1° gridded precipitation dataset from 1982 to 2005. Albeit use of the CPC data set is not ideal for fine spatial-scale analyses, it has been demonstrated to be suitable for investigating land surface processes at regional scales [e.g., Higgins et al., 1996; Gochis et al., 2006, 2007; Forzieri et al., 2013] and therefore is used here to quantify the interactions between ecosystem dynamics and precipitation. Figure 1b shows the CPC-derived percentage of annual precipitation during the July–September (JAS) period. The majority of the domain experiences a monsoon climate showing a strong seasonality with 50–80% of precipitation occurring during JAS and an average JAS precipitation gradient ranging from ~100 to 800 mm modulated by geographic position and elevation [e.g., Douglas et al., 1993; Vivoni et al., 2007, 2008;



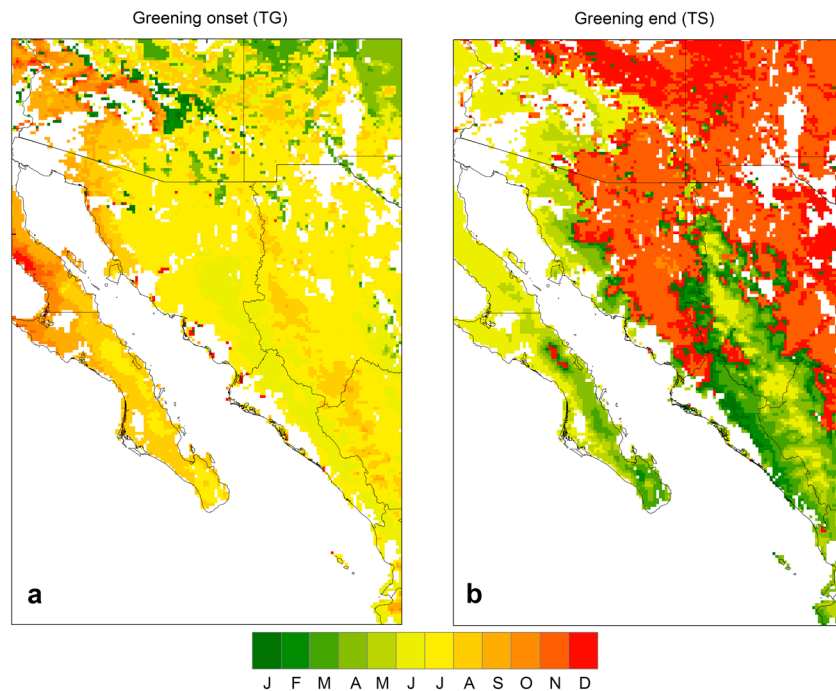


**Figure 3.** Interannual average (a) onset and (b) end of the greenness period. Areas with no NDVI seasonality or with an irrigation percentage greater than 10% are masked (white areas).

Forzieri *et al.*, 2011]. Note the increasing gradient of JAS precipitation (contour lines in Figure 1b) toward the southern, tropical areas of the North American Monsoon Region.

## 2.2. Retrieval of Time-Integrated NDVI, Monsoon Precipitation, and Rain-Use Efficiency

To describe vegetation dynamics, we use a set of metrics derived from the GIMMS data set as in Forzieri *et al.* [2011], namely, the onset (TG), end (TS), and duration (DUR) of the greenness period, and the time-integrated NDVI (TINDVI) used here as an estimate of NPP. Figure 2 shows the methodology for computing the various vegetation phenological metrics. First, 16 day NDVI values are scaled to range from 0 to 1 ( $NDVI_{ratio}$ ) through min-max normalization. Then, the greenness period is identified using a threshold approach, in which TG and TS are defined as the times when the scaled NDVI crosses a threshold value of  $T_n = 0.3$ , and DUR is the time period between TG and TS. TINDVI is calculated as the integrated NDVI (area below the curve) between TG and TS as follows:

$$TINDVI = \int_{TG}^{TS} NDVI(t)dt - [NDVI(TG) + NDVI(TS)]DUR/2. \quad (1)$$

Figures 3a and 3b show the interannual average of the onset (TG) and end (TS) of the greenness period over the study area. Pixels with seasonal NDVI variance lower than 0.03 (non-vegetated areas of Sonoran and Chihuahuan Deserts) or with more than 10% of irrigated areas (agricultural lands along the Mexican Pacific Coast and Colorado River) are masked and excluded from the analysis (inland white areas in Figure 3). Such screening procedures allow focusing on seasonal vegetation dynamics which are largely dominated by natural climate variability. Given the prevalent monsoon regime, vegetation greenness occurs mainly in the summer season (JAS), with the exception of parts of the Sonoran Desert (SD) which are also subject to a Mediterranean climate with a winter growing phase in Baja California.

To assess the suitability of time-integrated NDVI (TINDVI) as proxy of net primary productivity, we performed a correlation analysis in terms of Spearman rank ( $r_k$ ) between NPP ground measurements and the corresponding time-integrated NDVI values at the LTER sites. In this comparison, we implicitly assume that annual NPP relate primarily to the summer (monsoon) season. The correlation analysis included all annual estimates of the 10 LTER sites (even those outside North American Monsoon Region) to better test

the TINDVI capability to capture the interannual variability of NPP (119 pairs of observed/modeled annual NPP values). A similar correlation analysis was performed on the whole EMDI data set and separately on the sites with climatic conditions and biomes similar to those observed within the North American Monsoon Region. For this purpose, we selected sites with annual precipitation amount up to 1200 mm and annual average temperature lower than 15°C, as recorded in the EMDI data set. Then, by referring to the two different biome categories used in the EMDI data set, we focused on sites of (1) deciduous broadleaf forest/tropical, desert, evergreen needleleaf forest/temperate, grassland/C4 temperate, and savanna/temperate and (2) arid shrubland, closed and open shrubland, deciduous and evergreen forests, grass, savanna, subtropical forest, wooded grassland, woodland, and xeric forest. Note that time-integrated NDVI is valid over the large field of view of the AVHRR sensor ( $8 \times 8 \text{ km}^2$ ) which partially masks local-scale vegetation patterns and their controls [Noy-Meir, 1973; Le Houérou, 1984; Paruelo *et al.*, 1999]. As additional validation, we analyzed the Spearman rank between the MODIS-derived NPP and the AVHRR-derived time-integrated NDVI for the 2000–2006 period. First, MODIS-NPP was upscaled to 8 km to match the AVHRR spatial resolution. Then, the correlation analysis was performed at a pixel level over the North American monsoon domain (20 to 35°N, 105 to 115°W) using the 7 year average values to reduce the influence of possible modeling artifacts in the MODIS-NPP temporal evolution [Samanta *et al.*, 2011]. We point out that validation of AVHRR-TINDVI on MODIS-NPP products is not necessarily an independent test, as AVHRR-NDVI and MODIS-fPAR are derived from a similar set of surface reflectances but nevertheless serves to determine the feasibility of TINDVI as a proxy for NPP. Note that ground measurements of NPP are usually expressed in  $\text{gC/m}^2 \text{ yr}$ , whereas the unit of measure of TINDVI is days. We did not apply any conversion function to avoid introducing additional biases and uncertainty in the procedure and to facilitate the comparison of TINDVI with similar indices developed in the literature based on the integral of NDVI.

In water-controlled environments, ecosystems might have multiple greening periods depending on precipitation [Tarhule and Lamb, 2003; Dai *et al.*, 2004]. In the ecoregions within the North American Monsoon Region Forzieri *et al.* [2013] quantified the temporal lag between precipitation and vegetation greenness for winter (Mediterranean climate) and summer (monsoonal climate) periods. Here we focus only on the main greening period during the monsoon. We define the amount of precipitation (monsoon precipitation,  $P_r$ ) as the rainfall occurring between the onset of the greenness (TG)—shifted in advance by a given temporal lag ( $h$ )—and the end of the greenness (TS) as (Figure 2):

$$P_r = \int_{TG-h}^{TS} P dt, \quad (2)$$

where  $P$  is the CPC daily precipitation disaggregated to 8 km to match the vegetation data set and  $h$  is set to 75 days, a time span prior to the onset of the greening period (mainly in late spring) during which precipitation affects vegetation dynamics in most of the North American Monsoon Region [Forzieri *et al.*, 2013]. Thus,  $h$  represents the time lag of ecosystem responses to the occurrence of rainfall events. Such component has been quantified through an analysis of the correlation structures of remotely sensed vegetation dynamics with precipitation by Forzieri *et al.* [2013] and termed *biophysical memory* to refer to the ecosystem-specific abilities to retain a memory of a past climate signal. Intensive water users in desert and subtropical and tropical ecosystems (i.e., TDF, GSS, SD, and CD) usually develop a dense network of shallow roots to absorb moisture from small rainfall events [Rodríguez-Iturbe *et al.*, 2001] and are therefore more sensitive to the occurrence of early precipitation in the monsoon season. In contrast, mountain woodlands and conifer forests (i.e., EDF and CF), due to their ability to reach deeper soil water resources, are less influenced by monsoon precipitation variability, provided that a certain amount of water is available [Camberlin *et al.*, 2007]. These extensive water users are likely affected by soil moisture conditions at the start of the monsoon that depends on winter and spring precipitation [e.g., Swetnam and Betancourt, 1998; Rodríguez-Iturbe *et al.*, 2001; Williams *et al.*, 2012]. Since the concept of biophysical memory is relatively new, we assess the sensitivity of the study results to variations in  $h$ .

Rain-use efficiency (RUE) expresses the amount of net primary productivity produced in response to a unit of precipitation, usually referred to as the mean annual precipitation [e.g., Varnamkhasti *et al.*, 1995; Nicholson *et al.*, 1998; Prince *et al.*, 1998, 2008; Bai *et al.*, 2008a]. In our analysis, time-integrated NDVI

(TINDVI) is used as proxy of NPP, while Pr is the monsoon precipitation contributing to vegetation growth. Thus, rain-use efficiency is expressed in d/mm as follows:

$$\text{RUE} = \frac{\text{TINDVI}}{\text{Pr}}. \quad (3)$$

We contend that considering monsoon precipitation (Pr) instead of the mean annual precipitation (MAP), as in prior studies, may improve the understanding of vegetation-climate relations in ecosystems that are strongly influenced by a seasonal regime. To corroborate this, we compared relations of interannual variability between vegetation and precipitation calculated by using both mean annual and monsoon precipitation. An alternative way of estimating the rain-use efficiency is to equate it to the slope of the NPP-precipitation relationship ( $\text{NPP} = a + b(\text{MAP})$ ), for example, in *Paruelo et al.* [1999], *Lauenroth et al.* [2000], and *Huxman et al.* [2004]. However, *Verón et al.* [2005] noted that this slope represents an indicator of the sensitivity of NPP to changes in precipitation and does not exactly correspond to the efficiency of rainfall utilization unless the intercept to the regression equation is 0 (i.e.,  $\text{RUE} = b$  only if  $a = 0$ ), which seldom happens in ecosystems [*Paruelo et al.*, 1999]. Differences between the two methods tend to reduce as the rainfall amount increases [*Verón et al.*, 2005].

### 2.3. Analysis of Ecosystem Response to Precipitation Variability

We restricted our analysis to the period of 1982–2004 to account for the same number of phenological cycles and corresponding monsoon precipitation seasons in the North American Monsoon Region. Thus, spatiotemporal patterns of monsoon precipitation, time-integrated NDVI, and rain-use efficiency were calculated at the pixel scale for each year, resulting in 23 year time series. To investigate time-integrated NDVI and rain-use efficiency patterns across the precipitation gradient, we grouped pixels for each ecoregion type into interannual-averaged monsoon precipitation classes with a 50 mm interval (e.g., 75–125 mm, 125–175 mm, and 175–225 mm). To capture a representative ecosystem behavior, we focus on precipitation bins that contain at least 50 pixels. For each monsoon precipitation class, the spatially averaged values of time-integrated NDVI and rain-use efficiency were calculated. Corresponding spatial average values of DEM-derived elevation were also calculated for the classes to assess possible altitudinal controls on time-integrated NDVI and rain-use efficiency.

Interannual variations were quantified at the pixel scale within each ecoregion through the coefficient of variation (CV) defined as the interannual standard deviation divided by the interannual average. The interannual variability in time-integrated NDVI and monsoon precipitation were assumed to be related if the Spearman rank between the CVs were statistically significant (0.05 significance level). The dependence of the CV of time-integrated NDVI on the average and standard deviation of monsoon precipitation was also examined to better characterize the vegetation response to water availability. We reproduced the same analysis of interannual variability considering mean annual precipitation in place of monsoon precipitation, to verify possible differences in the sensitivity of the ecosystem responses. We point out that the aforementioned analysis explores the linkage between interannual variations of time-integrated NDVI and monsoon precipitation in the space dimension. The Spearman rank is calculated over all the pixels, each characterized by specific interannual variations. To better characterize the time dimension of such relations, the original data set of annual estimates of time-integrated NDVI and monsoon precipitation (1982–2004) was split in two subsets including the first and last 12 years of observations (1982–1993 and 1993–2004), respectively. Then, the analysis of the Spearman rank was replicated on the CV values calculated separately for the two temporal subsets. Changes in the strength of correlations between time-integrated NDVI and monsoon precipitation amongst the two different subsets may explain how their interannual relations evolve in time.

Long-term trends over the 23 year record were assessed both at the pixel and ecoregion level. For the latter, ecoregion spatial averages of monsoon precipitation, time-integrated NDVI, and rain-use efficiency were calculated using the corresponding pixel values. Trends in the ecoregion-averaged values were assessed through a Mann-Kendall test with a 0.05 significance level. At the pixel scale, linear trend tests were performed. Recent studies have demonstrated that GIMMS data are capable of capturing long-term dynamics of semiarid regions, whereas analysis in arid zones should be viewed with caution due to larger uncertainties of the NDVI signal [*Fensholt and Proud*, 2012; *Fensholt et al.*, 2012]. We point out that pixels with no vegetation are excluded from our analysis, and the approach based on seasonal NDVI

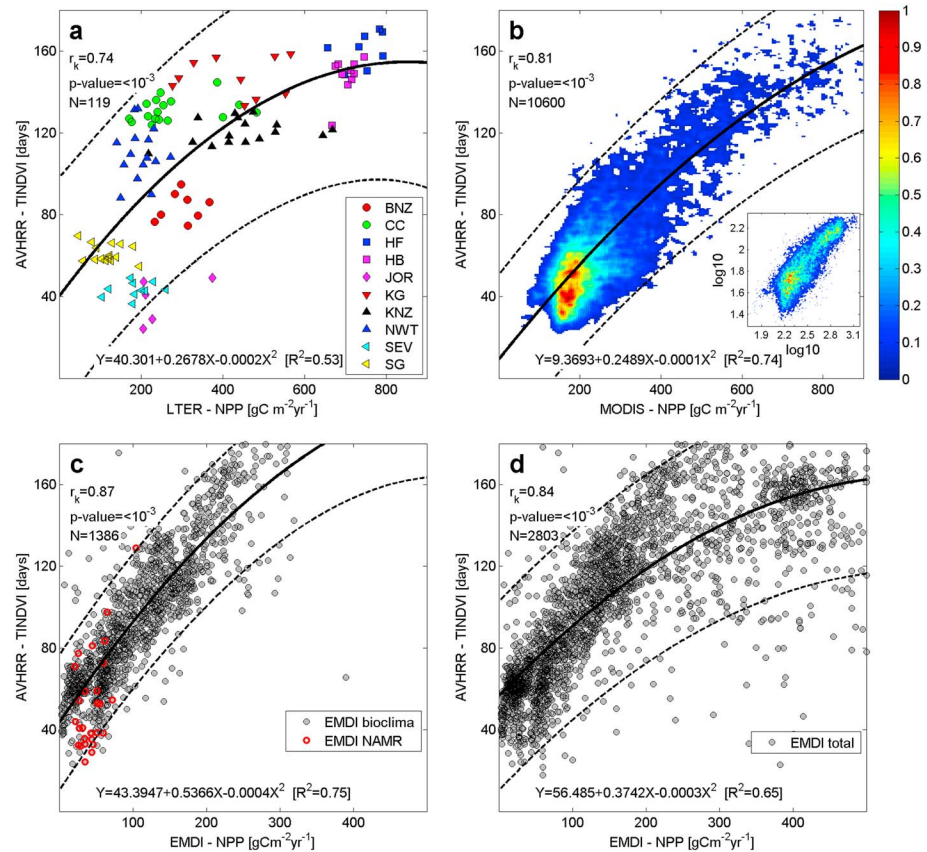


**Figure 4.** (a) Scatterplot between annual values of field measured NPP at LTER sites (labeled LTER-NPP) and corresponding time-integrated NDVI at the collocated pixels. (b) Normalized two-dimensional frequency distribution of remotely sensed NPP from MODIS (labeled MODIS-NPP) and time-integrated NDVI pixels, with colors indicating increasing density of pixels; same values are shown in log-log scale in the inset. (c) Scatterplot between annual average values of NPP values at EMDI sites (labeled EMDI-NPP) with bioclimatic conditions similar to those observed in the North American Monsoon Region and corresponding time-integrated NDVI at the collocated pixels (EMDI bioclimate); EMDI sites within the study domain are shown in red circles (EMDI-NAMR). (d) Scatter plot between annual average values of NPP values at the total EMDI sites (labeled EMDI-NPP) and corresponding time-integrated NDVI at the collocated pixels (EMDI total). Statistical measures (Spearman rank  $r_k$ ,  $p$  values, and sample size  $N$ ) are reported in the panels.

integrals is robust since the seasonal variations of NDVI have been extracted based on a phenological approach calibrated on the North American monsoon ecosystems [Forzieri *et al.*, 2011]. Thus, we believe that possible uncertainties of the NDVI signal in sparsely vegetated areas [Huete *et al.*, 1985] do not affect significantly our trend analysis.

Sensitivities of interannual average, CV, and long-term trends of monsoon precipitation were calculated at the pixel scale for varying  $h$  within the 0–6 month range and then aggregated at the ecoregion level.

### 3. Results

#### 3.1. Validation of Time-Integrated NDVI-Derived Proxy for NPP

To build confidence in the use of time-integrated NDVI (TINDVI) as a proxy for NPP, Figure 4 compares the proposed approach against three different validation data sets that convey complementary information: multiple annual observations at the LTER sites are useful to assess the NPP interannual variability, while EMDI and MODIS allow a more robust analysis of the spatial patterns of vegetation. Figure 4a is a scatterplot between NPP obtained from field observations at the LTER sites and the time-integrated NDVI at the corresponding AVHRR pixel, for all available annual observations ( $N = 119$ ). A correlation analysis showed a good agreement between LTER-NPP and AVHRR-TINDVI with a significant Spearman rank of 0.74 ( $p < 10^{-3}$ ). Figure 4b shows a frequency distribution of remotely sensed MODIS-NPP and AVHRR-TINDVI at collocated



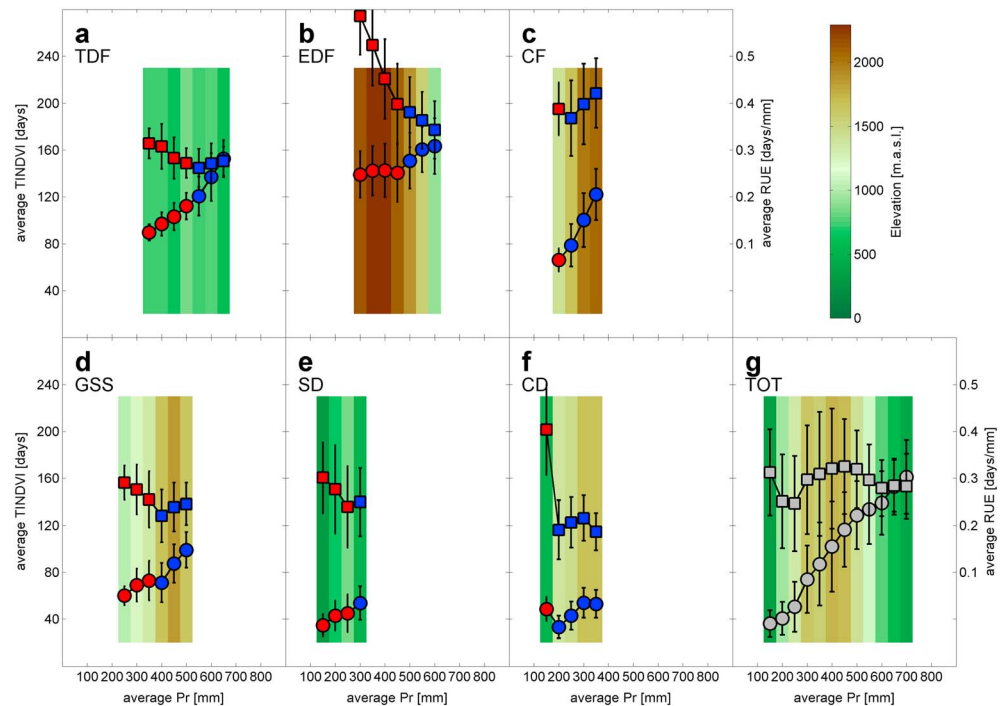


**Figure 5.** Relations between the interannual average monsoon precipitation (Pr) and interannual average and standard deviation of time-integrated NDVI (TINDVI, circles and bars, left y axis) and interannual average and standard deviation of rain-use efficiency (RUE, squares and bars, right y axis) for (a–f) each ecoregion and (g) for the total area (TOT). Red and blue colors in time-integrated NDVI and rain-use efficiency profiles are used to identify possible dry and wet elevation bands in each ecoregion. Spatial averages of elevation in each monsoon precipitation bin are overlaid in shaded colors.

pixels in the North American Monsoon Region. A correlation analysis revealed a highly significant correspondence between the two data sets with a Spearman rank of 0.81 ( $p < 10^{-3}$ ,  $N = 10,600$ ). Figures 4c and 4d show scatterplots between NPP obtained from EMDI sites and the time-integrated NDVI at the corresponding AVHRR pixel, for EMDI sites with bioclimatic conditions similar to those of the North American Monsoon Region (EMDI bioclimate) and for all available sites (EMDI total). Note that EMDI sites within the North American Monsoon Region are shown in red circles in Figure 4c (EMDI-NAMR) and are included in the EMDI bioclimate subset. The correlation results exhibit a highly significant agreement between EMDI-NPP and AVHRR-TINDVI with a Spearman rank of 0.87 ( $p < 10^{-3}$ ,  $N = 1386$  for EMDI bioclimate) and 0.84 ( $p < 10^{-3}$ ,  $N = 2803$  for EMDI total).

Quadratic regression functions and confidence bounds are overlaid in each panel to better interpret the TINDVI/NPP relations in space and time. Spatial patterns of NPP appear to be well captured by time-integrated NDVI especially for North American monsoon ecosystems or similar worldwide biomes ( $R^2 = 0.74$  and  $R^2 = 0.75$  in Figures 4b and 4c, respectively). A larger uncertainty emerges in the TINDVI/NPP relation when multiple annual observations and different biomes are included in the regression analysis ( $R^2 = 0.53$  and  $R^2 = 0.65$  in Figures 4a and 4d, respectively). This is likely due to limitations of the AVHRR sensor to synthesize fine-scale determinants of soil water availability and physiological processes whose temporal variations may have important effects on NPP [Noy-Meir, 1973; Le Houérou, 1984; Paruelo et al., 1999]. The intrinsic uncertainty of year-to-year NPP measurements as well as the limitations of spectral reflectances to synthesize phenological dynamics in certain biomes, such as tundra and croplands, may furthermore complicate the validation process on interannual scale and across a larger variety of biomes [Clark et al., 2001; Gobron et al., 1998].

The nonlinear relationship of TINDVI/NPP is more evident when a larger productivity range is explored (Figures 4a and 4d). Results show a stronger variation in time-integrated NDVI with NPP for ecosystems with low NPP, mainly dominated by grasslands (JOR, SEV, SG, and BNZ in Figure 4a), and a weaker variation of time-integrated NDVI with NPP for higher productivity ecosystems consisting of croplands and mixed deciduous forests (HF, CC, NWT, KG, HB, HF in Figure 4a). This is likely related to the saturation effects of NDVI

**Table 1.** Description of Time-Integrated NDVI (TINDVI) and Rain-Use Efficiency (RUE) Variations Along the Monsoon Precipitation (Pr) Gradient for Dry and Wet Subareas in Each Ecoregion

Ecoregion		Subareas	
		Dry	Wet
TDF	Tropical dry forests of the Pacific coastal plain, hills, and canyons	400 mm $\leq$ Pr $\leq$ 500 mm TINDVI: linear increase RUE: linear decrease	500 mm $<$ Pr $\leq$ 750 mm TINDVI: linear increase (steeper) RUE: linear increase
EDF	Sierra Madre Occidental mountain woodlands composed of evergreen and deciduous forests	300 mm $\leq$ Pr $\leq$ 450 mm TINDVI: steady behavior RUE: linear decrease	450 mm $<$ Pr $\leq$ 600 mm TINDVI: linear increase RUE: linear decrease
CF	Conifer forests in Arizona and New Mexico	Pr $\leq$ 200 mm (only one bin)	200 mm $<$ Pr $\leq$ 350 mm TINDVI: linear increase RUE: linear increase after jump discontinuity
GSS	Semiarid grasslands, shrublands, and subtropical scrublands in the Sierra Madre Occidental piedmont	250 mm $\leq$ Pr $\leq$ 350 mm TINDVI: linear increase RUE: linear decrease	350 mm $<$ Pr $\leq$ 600 mm TINDVI: linear increase (steeper) RUE: linear increase
SD	Sonoran Desert	150 mm $\leq$ Pr $\leq$ 250 mm TINDVI: linear increase RUE: linear decrease	250 $<$ Pr (only one bin)
CD	Chihuahuan Desert	Pr $\leq$ 150 mm (only one bin)	150 mm $<$ Pr $\leq$ 450 mm TINDVI: linear increase after local minima at 200 mm Pr RUE: concave behavior (local maxima at 300 mm)

beyond a certain biomass density, as observed on multilayer vegetation and canopy structures with high leaf area index, such as forests and agricultural crops [e.g., Sellers, 1985; Gobron *et al.*, 1998].

Furthermore, other phenomena, such as the dependence of light use efficiency from the fraction of diffuse radiation, cannot be properly synthesized by visible and near-infrared spectral indexes [Knobl and Baldocchi, 2008]. However, we point out that most North American monsoon ecosystems and worldwide sites with analogous bioclimatic conditions fall within the lower NPP values, from 100 to 300 gC/m<sup>2</sup> yr (Figures 4a–4c). Since time-integrated NDVI is strongly linked in a linear fashion to NPP for these low values of NPP, inferences based on time-integrated NDVI can be reasonably translated to NPP. While the relation between NDVI and NPP has been viewed with caution for certain biomes [Knapp and Smith, 2001], our results support the use of time-integrated NDVI to assess primary productivity in the North American Monsoon Region.

### 3.2. Time-Integrated NDVI and Rain-Use Efficiency Variations Across the North American Monsoon Precipitation Gradient

Based on the above mentioned validation, we explored the variation of time-integrated NDVI and rain-use efficiency as a function of the precipitation gradient in the North American Monsoon Region and the six major ecoregions. Figure 5 shows relations between the interannual average monsoon precipitation (Pr) with respect to the interannual average and standard deviation of time-integrated NDVI (TINDVI) and rain-use efficiency (RUE). The relations are based on the spatial maps shown in Figure S1 in the supporting information and are complemented with statistics calculated at the ecoregion scale in Table S1 in the supporting information. Note that the monsoon precipitation for the NAMR ranges from 100 to 800 mm across its regional gradient, while each ecoregion exhibits a smaller range of monsoon precipitation due to the minimum number of 50 pixels required per bin and their varying precipitation characteristics. We also identify dry and wet subareas in each ecoregion (as red and blue symbols) and show their corresponding locations in Figure S2 in the supporting information (as red and blue areas). These subareas were determined in each ecoregion based on the functional variation of time-integrated NDVI and rain-use efficiency with monsoon precipitation shown in Figure 5.

In general, all ecoregions show an increase in time-integrated NDVI and decrease in rain-use efficiency with increased monsoon season precipitation. However, the shapes (e.g., slope, convexity, and discontinuities) of the profiles characterizing the variation of time-integrated NDVI and rain-use efficiency with monsoon precipitation differ strongly across the ecoregions. Table 1 provides details of the functional variation for each ecoregion for the dry and wet subareas. Tropical dry forests (TDF), semiarid grasslands, shrubland, and scrublands (GSS), and desert environments (SD and CD) show a prevalently linear dependence of time-

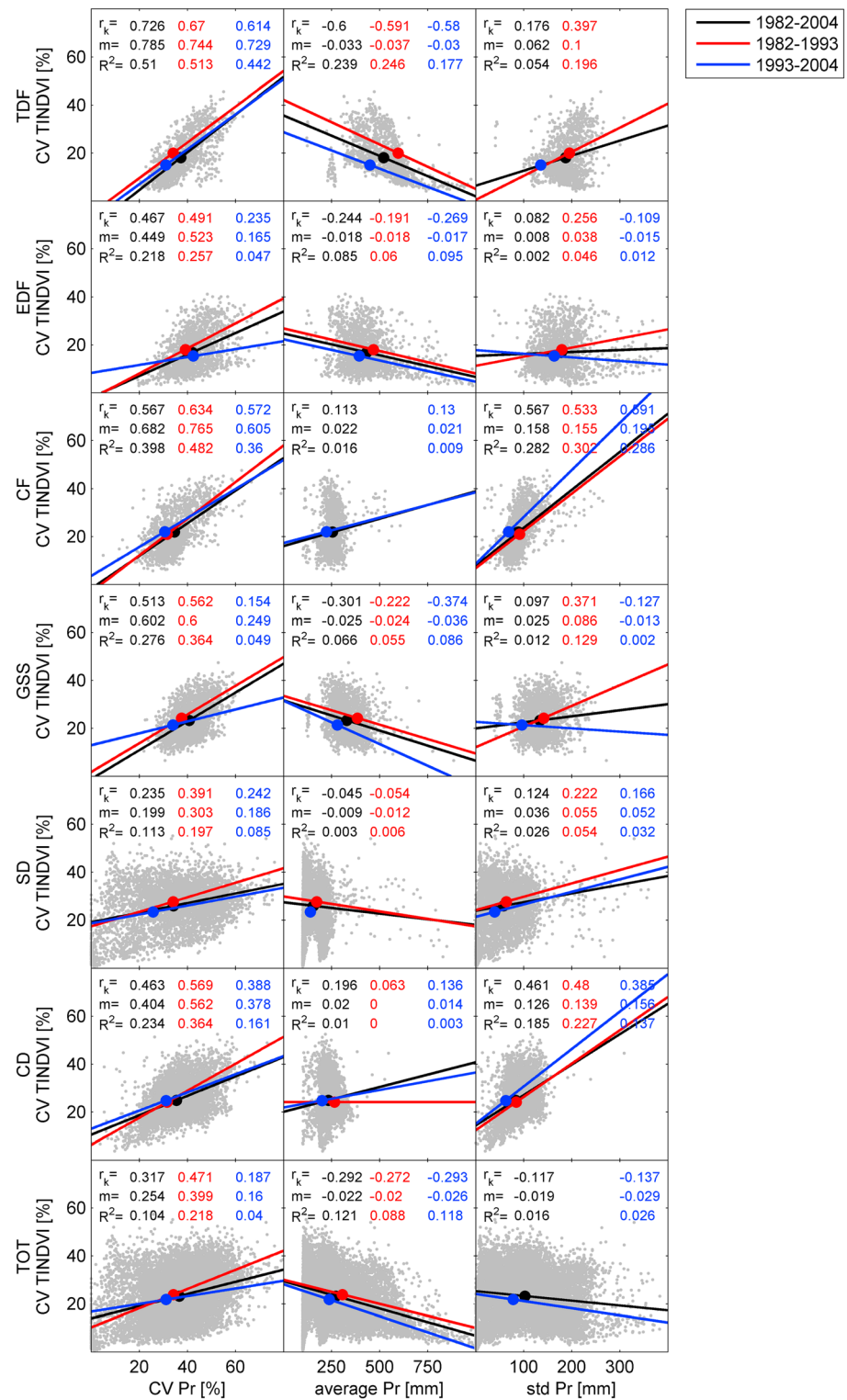


**Figure 6.** Scatter plots between interannual CV of time-integrated NDVI (TINDVI) and monsoon precipitation (Pr) metrics (CV, average and standard deviation in the first, second, and third columns, respectively) for each ecoregion and the North American Monsoon Region (TOT, seventh row). Analysis performed on the whole time series (1982–2004) are shown by pixel-specific interannual values as gray dots, fitted linear regressions as black lines, and the mean values as black dots. Statistical measures (Spearman rank  $r_k$ , slope of the regression line, and coefficient of determination  $R^2$ ) are shown in panels. Results for the first (1982–1993) and last (1993–2004) temporal subsets are shown in red and blue colors, respectively.

integrated NDVI (circles) and rain-use efficiency (squares) on monsoon precipitation. Interestingly, profiles in tropical dry forests (TDF) and semiarid grasslands, shrubland, and scrublands (GSS) switch from a decreasing trend to an increasing trend of rain-use efficiency with monsoon precipitation above 500 mm and 350 mm, respectively (e.g., wet subarea), corresponding to steeper positive time-integrated NDVI gradients in each case. A similar relative increase in rain-use efficiency is also distinct in Sonoran and Chihuahuan Deserts (SD and CD). In contrast, evergreen and deciduous forests (EDF) exhibit a constant profile of time-integrated NDVI and a corresponding linear reduction in rain-use efficiency for monsoon precipitation below 500 mm (dry subarea). For wetter conditions, evergreen and deciduous forests (EDF) experiences a steeper linear increase in time-integrated NDVI (linear decrease in rain-use efficiency), which is also partially discernible in conifer forests (CF, wet subarea). The low explained variances (up to 2%) in elevation-precipitation linear regression models calculated separately for each ecoregion suggest that elevation may, in fact, play an important role in explaining the variations of time-integrated NDVI and rain-use efficiency along the precipitation gradient. This is exemplified by the consistent features of time-integrated NDVI and rain-use efficiency with elevation in Figure 5 and quantified by modest, but significant, correlation coefficients (up to 0.4, calculated over all pixels in each ecoregion). The positive effect of elevation is particularly evident in semiarid grasslands, shrubland, and scrublands (GSS) and conifer forests (CF) which show consistent increases in time-integrated NDVI and rain-use efficiency at higher elevation sites (Figure S2 in the supporting information).

Spatial averages across all ecoregions shown in Figure 5g (total area (TOT)) synthesize two of the main time-integrated NDVI and rain-use efficiency variations with precipitation that have been reported previously: (1) TINDVI-derived NPP primarily increases with increasing precipitation, while rain-use efficiency decreases weakly [e.g., Huxman *et al.*, 2004], and (2) an intermediate peak of rain-use efficiency emerges in correspondence of a steeper gradient of time-integrated NDVI occurring between 300 and 550 mm precipitation [e.g., Paruelo *et al.*, 1999], which partially obscures the overall decreasing trend between rain-use efficiency and monsoon precipitation. Correlation between elevation and rain-use efficiency is also evident for the entire domain and varies across the monsoon precipitation gradient, with  $\sim 0.37$  correlation below 350 mm,  $\sim 0.44$  in the 350–550 mm range and up to 0.17 for higher monsoon precipitation, obtained over all pixels belonging to the sampled precipitation interval.

### 3.3. Interannual Variability in Time-Integrated NDVI and Monsoon Precipitation

Figure 6 presents the relationships between the interannual variability in time-integrated NDVI (shown as the CV TINDVI) and the interannual metrics of monsoon precipitation (CV, average and standard deviation Pr) for each ecoregion and the entire North American Monsoon Region (labeled TOT). Statistical metrics, including the Spearman rank ( $r_k$ ), the slope of the regression line, and coefficient of determination ( $R^2$ ) are also reported. Results for the whole data set (1982–2003) and the first (1982–1993) and last (1993–2003) temporal subsets are shown in black, red, and blue colors, respectively. Linear regressions are displayed for significant correlations ( $p < 0.05$ ). Focusing first on the whole data set, the analyses reveal a significant positive correlation ( $p < 10^{-3}$ ) between the CV of time-integrated NDVI and the CV of monsoon precipitation for all six ecoregions (with  $R^2$  ranging from 0.11 to 0.51), indicating that the interannual variations in net primary productivity (using time-integrated NDVI as a proxy) are strongly linked to the corresponding variations in monsoon precipitation. High-elevation woodlands (EDF and CF) and grasslands, shrublands, and tropical ecosystems (GSS and TDF) are characterized by stronger correlations than desert environments (SD and CD). Deserts also exhibit higher mean CV of time-integrated NDVI (black dots) as compared to other ecoregions. The strength of the correlation between the CVs of time-integrated NDVI and monsoon precipitation is explained by how the CV of time-integrated NDVI decreases with the average of monsoon precipitation and increases with the standard deviation of monsoon precipitation, as visualized by the primarily negative and positive slopes in the second and third columns, respectively. A similar comparison between CV of time-integrated NDVI and annual precipitation metrics (Figure S3 in the supporting information) revealed much lower correlations, reinforcing the importance of quantifying the growing-season precipitation to explore vegetation-climate relations in seasonal regimes.

Interannual average and standard deviation of monsoon precipitation contribute differently in explaining the ecosystem response to precipitation variability, as expressed through their respective correlations with the CV of time-integrated NDVI. In wetter ecoregions with average monsoon precipitation (Pr) larger than



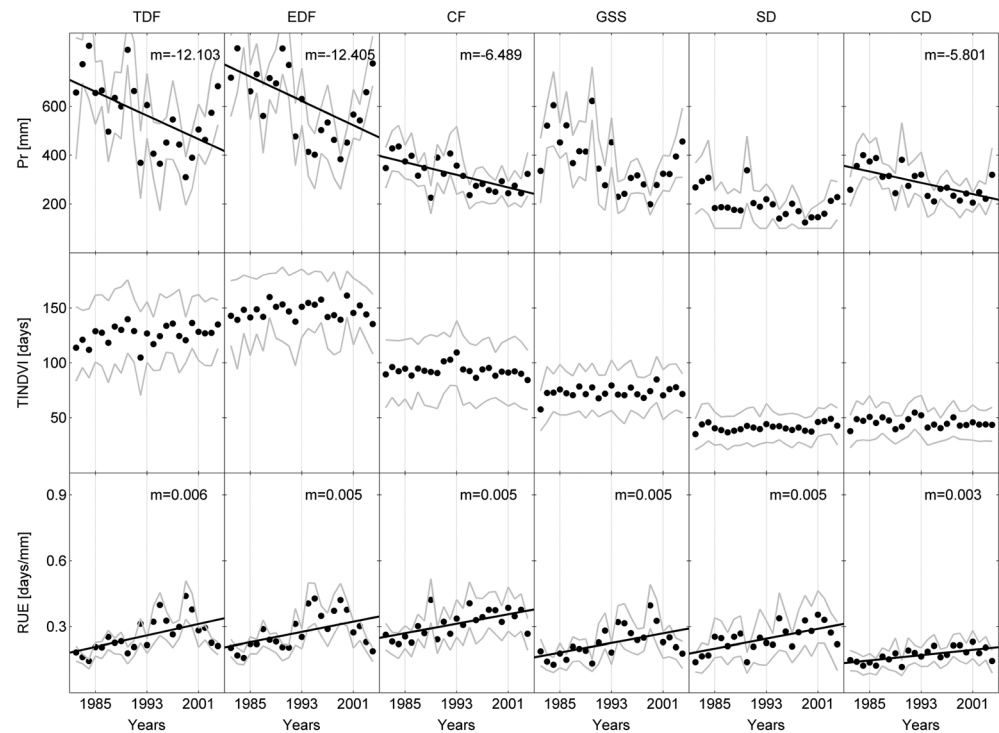


**Figure 7.** Long-term variations of ecoregion-averaged monsoon precipitation (Pr), time-integrated NDVI (TINDVI), and rain-use efficiency (RUE) with statistically significant linear trends shown as black lines and slopes ( $m$ ) indicated in the panels. The 80th and 20th percentiles in each ecoregion are shown as upper and lower gray lines.

~350 mm (mainly tropical dry forests (TDF), evergreen and deciduous forests (EDF), and semiarid grasslands, shrubland, and scrublands (GSS)), the link between time-integrated NDVI and precipitation is mainly driven by variations in average monsoon precipitation, as suggested by higher correlations between CVs of time-integrated NDVI and average monsoon precipitation, as compared to those between CVs of time-integrated NDVI and standard deviation of monsoon precipitation (Figure 6). Opposite correlation patterns are observed in drier ecosystems (CF, SD, and CD).

Focusing on results for the first and last 12 year periods, we note that for all the North American monsoon ecosystems the link between CVs time-integrated NDVI and monsoon precipitation tends to evolve in time. In particular, the Spearman rank ( $r_k$ ), slope of the regression line ( $m$ ), and coefficient of determination ( $R^2$ ) of CV of time-integrated NDVI and the CV of monsoon precipitation are significantly lower in 1993–2004 as compared to those observed in 1982–1993 (first column of Figure 6). Smoother slopes of regression lines in 1993–2004 exemplified a weaker connection of interannual variations of time-integrated NDVI to the corresponding variations in monsoon precipitation with respect to the previous period.

### 3.4. Long-Term Trends in Monsoon Precipitation, Time-Integrated NDVI, and Rain-Use Efficiency

Long-term trends of ecoregion-averaged monsoon precipitation (Pr), time-integrated NDVI (TINDVI), and rain-use efficiency (RUE) are shown in Figure 7 in addition to the 20th and 80th percentiles of each distribution (gray lines). Linear regressions (black lines) are displayed for significant linear trends ( $p < 0.05$ ) using the Mann-Kendall test, and corresponding slopes ( $m$ ) are reported. Over the period of 1982–2004, monsoon precipitation significantly decreased over tropical dry forests (TDF), evergreen deciduous forests (EDF), conifer forests (CF), and the Chihuahuan Desert (CD) ecoregions, ranging from ~5 to 12 mm/yr in reduction. Time-integrated NDVI, on the other hand, does not show a significant trend when averaged over an entire ecoregion for any ecosystem, consistent with studies by Forzieri *et al.* [2011] and Fensholt *et al.* [2012]. Nevertheless, in combination with decreasing monsoon precipitation trends, a statistically significant increase in rain-use efficiency is observed for all ecoregions, from 0.003 to 0.006 d/mm/yr increase. The high interannual variability in rain-use efficiency that is evident for all ecoregions is clearly linked to monsoon precipitation.

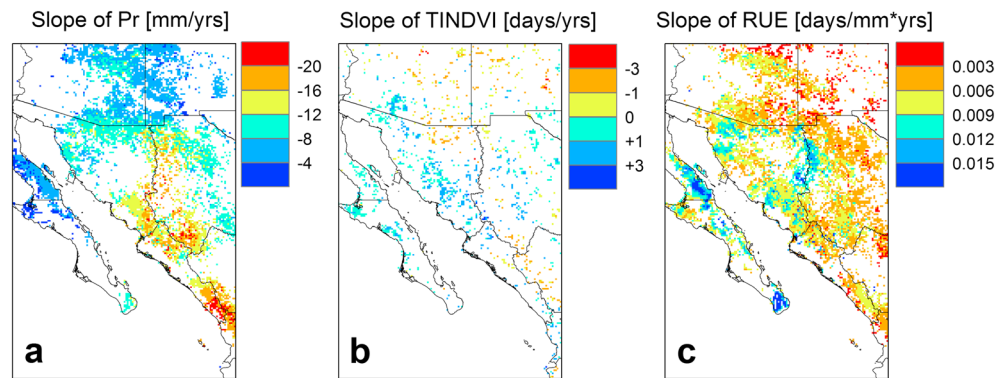


**Figure 8.** Spatial maps of the linear trends of interannual variations for individual pixels in (a) monsoon precipitation (Pr), (b) time-integrated NDVI (TINDVI), and (c) rain-use efficiency (RUE). White pixels represent areas where the Mann-Kendall test for a linear trend is not satisfied at the 0.05 significance level.

To further explore these long-term variations, Figure 8 presents the slopes of significant linear trends of monsoon precipitation, time-integrated NDVI, and rain-use efficiency for individual pixels. This is complemented by Table 2 which presents the percentage of pixels in each ecoregion experiencing significant positive or negative linear trends. Most ecoregions have large areas characterized by significant negative monsoon precipitation trends ( $S_{Pr}$ , Figure 8a). A marked latitudinal variation is observed with greater reductions in monsoon precipitation toward the wetter southern areas (compare to Figure S1a in the supporting information). The spatial patterns of positive and negative linear trends in time-integrated NDVI ( $S_{TINDVI}$ , Figure 8b) illustrate why the ecoregion averages revealed no significant trend. Nevertheless, at the individual pixel scale, time-integrated NDVI does have significant changes that tend to increase the areas with positive rain-use efficiency trends above that solely attributed to monsoon precipitation, in particular for tropical dry forests (TDF), semiarid grasslands, shrubland, and scrublands (GSS), and Sonoran Desert (SD) ecoregions (Table 2). This suggests that time-integrated NDVI increases in these ecoregions are occurring at the same time as a decreasing trend in monsoon precipitation. This is exemplified by large areas experiencing positive rain-use efficiency trends ( $S_{RUE}$ ) over most of the North American Monsoon Region and hot spots with larger positive slopes over Baja California (SD, TDF, and EDF) and along the Sonora and Chihuahua borders (CF, EDF, and TDF, Figure 8c).

### 3.5. Sensitivity of Monsoon Precipitation to Biophysical Memory

We assess the sensitivity of the study results to variations in biophysical memory,  $h$ . We focused on the influence of the temporal lag ( $h$ ) on the interannual average, CV, and long-term trends of monsoon precipitation (Pr) for each ecoregion in Figure S4 in the supporting information. Most of the variability in the precipitation metrics occurs within the 0 to 3 month range of  $h$ . This is particularly evident in evergreen and deciduous forests (EDF) where the late spring rainfall affects monsoon precipitation climatology. For increasing  $h$ , both average and standard deviations of monsoon precipitation tend to increase linearly at the same pace, except for the Sonoran Desert (SD) whose variability is linked to the considerable fraction of winter-spring

**Table 2.** Percentage of Pixels in Each Ecoregion With Significant Linear Trends (Positive and Negative) of Monsoon Precipitation (Pr), Time-Integrated NDVI (TINDVI), and Rain-Use Efficiency (RUE)

Ecoregion		$S_{Pr}$		$S_{TINDVI}$		$S_{RUE}$	
		+	−	+	−	+	−
TDF	Tropical dry forests of the Pacific coastal plain, hills, and canyons	0	51	9	1	74	0
EDF	Sierra Madre Occidental mountain woodlands composed of evergreen and deciduous forests	0	40	3	4	47	0
CF	Conifer forests in Arizona and New Mexico	0	65	1	4	53	0
GSS	Semiarid grasslands, shrublands, and subtropical scrublands in the Sierra Madre Occidental piedmont	0	31	11	2	58	0
SD	Sonoran Desert	0	27	16	2	44	0
CD	Chihuahuan Desert	0	48	4	5	42	0

precipitation. Long-term trends in monsoon precipitation show progressively steeper slopes for increasing  $h$ , consistent with larger amount of available water. As depicted in Figure S4, the selection of  $h = 75$  days (2.5 months) as a temporal lag for the above analyses captures reasonably well the monsoon precipitation metrics across all tested values of  $h$  and thus suggests that the study results are robust with respect to the definition of monsoon precipitation.

## 4. Discussion

### 4.1. How Do Time-Integrated NDVI and Rain-Use Efficiency Change Along a Precipitation Gradient in the North American Monsoon Region?

Time-integrated NDVI and rain-use efficiency variations along the precipitation gradient and amongst different ecoregions indicate possible nonlinear mechanisms dependent on phenological processes. In particular, we distinguish two main ecosystem types which rely on intensive or extensive water use. Intensive users, such as tropical dry forests, semiarid grasslands, and desert environments, show a prevalent linear dependence of time-integrated NDVI on monsoon precipitation. Intensive users exhibit a reversal in the trend of rain-use efficiency with monsoon precipitation due to relatively enhanced ecosystem productivity in wetter subareas. This reinforces the concept that precipitation exerts a causal effect in water-controlled ecosystems and attributes it primarily to seasonal (monsoonal) rainfall [Schwinning and Sala, 2004]. Extensive users, such as evergreen and deciduous forests, mainly show constant profiles of time-integrated NDVI with increasing precipitation (steep linear decrease in rain-use efficiency), likely resulting from the combined effect of additional drivers, such as temperature and radiation [Nemani et al., 2003]. However, beyond a given precipitation threshold, vegetation tends to respond with a more vigorous productivity that is linearly related to seasonal precipitation. This corroborates that larger amounts of precipitation and deeper infiltration are needed to trigger intense vegetation productivity of deep-rooted plants, as stated in the theory of hierarchy of responses to resource pulses of Schwinning and Sala [2004].

Results based on the ecoregion averages support the transitional nature of vegetation and biogeochemical constraints on phenology. The former are associated to physiological characteristics of the dominant plants, while the latter are related to the magnitude of nutrient limitation. Our analysis, built on a remote sensing phenological approach of a set of different ecosystems, allows retrieving a spatially consistent and comprehensive picture of how the limiting factors of vegetation change along a large precipitation range. Such constraints have been observed singularly in previous literature and analyzed separately. At the dry end of the precipitation gradient, the high water use efficiency related to individual plant growth in desert and semiarid environments translates into high rain-use efficiency [e.g., Huxman et al., 2004]. Rain-use efficiency tends to progressively decrease in the range of 100 to 300 mm, while time-integrated NDVI increases at a small rate, due to the changes in vegetation constraints, such as a reduction in relative growth rates, increased density limitations, and coexistence of numerous species competing for water [Paruelo et al., 1999; Bai et al., 2008a]. Along the 300–550 mm range, higher rain-use efficiency values and the greater increase in time-integrated NDVI are observed primarily in evergreen and deciduous forests due to their typical deep-rooted plant morphology which allows for high photosynthetic activity even under relatively low monsoon precipitation [Forzieri et al., 2011, 2013]. At the wet end of the precipitation gradient, rain-use efficiency decreases again because plant growth is constrained by biogeochemical limits, such as nitrogen and light [Paruelo et al., 1999; Knapp and Smith, 2001; Huxman et al., 2004], and increasing monsoon precipitation tends to be partially depleted by other processes, such as runoff and percolation [Campos et al., 2013].

Time-integrated NDVI and rain-use efficiency appear to be positively influenced by elevation. This could be related to the reduction in atmospheric evaporative demand and increase in greenness duration at higher elevations [Forzieri et al., 2011] that may ultimately increase plant growth and promote a number of slower controlling processes, such as soil organic matter accumulation [Schwinning and Sala, 2004]. Dependence of rain-use efficiency on elevation could also reflect the influence of a set of abiotic and biotic factors varying across mountain fronts that ultimately affect leaf anatomical features such as the specific leaf area [Hulshof et al., 2013] or the stomatal conductance [Thomas, 2011]. In addition, lower temperatures in mountain areas allow for a larger portion of precipitation to become available for vegetation growth. Increases in species richness that have been found to be positively influenced by topography [Coblentz and Riitters, 2004] could additionally lead to larger rain-use efficiency due to a complementary use of water by different species [Yang et al., 2010].

#### 4.2. Are the Interannual Variations of Time-Integrated NDVI and Monsoon Precipitation Related?

Statistical analyses showed a significant positive correlation between interannual variations in time-integrated NDVI and monsoon precipitation across all ecoregions. In particular, vegetation in areas with low monsoon precipitation (dry subareas) tends to experience larger variability of vegetation response to seasonal rainfall fluctuations. These results are consistent with previous studies [Le Houérou, 1984; Fang *et al.*, 2001; Yang *et al.*, 2008] but contradict the absence of significant interannual precipitation control on vegetation dynamics found by Knapp and Smith [2001] and Goward and Prince [1995]. In regions with a pronounced seasonality, such as the North American Monsoon Region, the use of the effective (seasonal) precipitation contributing to the vegetation dynamics instead of the annual precipitation explains the differing outcomes from prior studies. Furthermore, precipitation climatology plays an important role in diversifying the relations between interannual vegetation productivity and interannual precipitation in the diverse ecoregions. At the wet end of the precipitation gradient, mainly over tropical dry forests and evergreen and deciduous forests, the interannual variations of vegetation responses depend on the total water availability. In contrast, at the dry end of the precipitation gradient, semiarid and desert environments are largely sensitive to the magnitude of the year-to-year changes in monsoon precipitation. This suggests that climatology of monsoon precipitation substantially modulates the capacity of plants to buffer interannual changes in precipitation.

Interestingly, we found that the sensitivity of the interannual variations of vegetation productivity to the monsoon precipitation declines with time. This may suggest an increase in the ecosystem water use efficiency and/or a growing importance of other environmental drivers of the interannual dynamics of productivity within the North American Monsoon Region.

#### 4.3. Is There Evidence of a Long-Term Signal Imposed on the Interannual Variability of Rain-Use Efficiency?

Based on the 23 year records, we identified long-term negative trends in monsoon precipitation (Pr), no long-term trends in time-integrated NDVI (TINDVI), and significant long-term positive trends in rain-use efficiency (RUE) at the ecoregion scale. These findings are in line with the progressive reduction of precipitation control on the year-to-year fluctuations of time-integrated NDVI as shown in the previous section and suggest an increased capacity of the vegetation to utilize precipitation inputs for photosynthetic activity. We recognize that quantifying trends in monsoon precipitation and time-integrated NDVI is necessary but not sufficient to fully understand changes in phenological dynamics. However, these trends may help in identifying the possible mechanisms sustaining the increasing rain-use efficiency trends. We hypothesize that the observed trends are the results of ecosystem acclimation to a gradual reduction in water availability and increase in CO<sub>2</sub> concentration, known as the CO<sub>2</sub> fertilization effect. Water availability from rainfall events represents a fundamental source for plant growth, while atmospheric CO<sub>2</sub> regulates the evapotranspiration process via stomatal control. A progressive reduction of water availability and an increased concentrations in CO<sub>2</sub> [Hartmann *et al.*, 2013] tend to reduce stomatal conductance, thus making plants less susceptible to dehydration and sustaining a more efficient rain use [Leakey *et al.*, 2009; Keenan *et al.*, 2013]. Isolating the direct biochemical role of CO<sub>2</sub> in long-term greening trends from other key resources (such as light, water, and nutrients [Field *et al.*, 1992]) and from socioeconomic factors, such as land use change [Houghton, 2003], is difficult. However, this complexity is reduced focusing on ecosystems where water plays the dominant role in primary production and where plant water use and photosynthesis are strictly connected [Donohue *et al.*, 2013]. Thus, our hypothesis of enhancement of photosynthesis due to rising CO<sub>2</sub> levels within the North American Monsoon Region seems plausible and is corroborated by the works of Donohue *et al.* [2013], which found analogous effects on the foliage cover in warm arid environments across the globe due to fertilization effect along the last decades. Similar combined effects of increasing CO<sub>2</sub> and hydrological stresses leading to increase in water use efficiency have been also observed on 35 tree ring sites of coniferous and deciduous species across Europe [Saurer *et al.*, 2014].

Adaptation strategies at the plant scale may also promote an optimized use of resources by maximizing the efforts for carbon assimilation (e.g., changes in leaf area index and in the root/shoot allocations) when faced with a reduction in water [Ogle and Reynolds, 2004; Reynolds *et al.*, 2004]. This supports a resilient behavior of water-limited ecosystems expressed by their capacity to cope with prolonged hydrological stresses, as also reported by Campos *et al.* [2013].



## Acknowledgments

We acknowledge funding from the NOAA Climate Program Office (grant CPPA GC07-019) and NOAA Earth System Science program (grant NA10OAR4310165) to E.R.V.

## References

- Alcaraz-Segura, D., E. Liras, S. Tabik, J. Paruelo, and J. Cabello (2010), Evaluating the consistency of the 1982–1999 NDVI trends in the Iberian Peninsula across four time series derived from the AVHRR sensor: LTDR, GIMMS, FASIR, and PALI, *Sensors*, *10*, 1291–1314.
- Asbjornsen, H., et al. (2011), Ecohydrological advances and applications in plant–water relations research: A review, *J. Plant Ecol.*, *4*(1–2), 3–22.
- Bai, Y., W. Jianguo, X. Qi, P. Qingmin, H. Jianhui, Y. Dianling, and H. Xingguo (2008a), Primary production and rain use efficiency across a precipitation gradient on the Mongolia plateau, *Ecology*, *89*(8), 2140–2153.
- Bai, Z. G., D. L. Dent, L. Olsson, and M. E. Schaepman (2008b), Global assessment of land degradation and improvement. 1. Identification by remote sensing, Report 2008/01, ISRIC World Soil Information: Wageningen, 79 pp.
- Beck, H. E., T. R. McVicar, A. I. J. M. van Dijk, J. Schellekens, R. A. M. de Jeu, and L. A. Bruijnzeel (2011), Global evaluation of four AVHRR-NDVI data sets: Intercomparison and assessment against Landsat imagery, *Remote Sens. Environ.*, *115*, 2547–2563.
- Brown, E. D. (1994), *Biotic Communities: Southwestern United States and Northwestern Mexico*, 342 pp., University of Utah Press, Salt Lake City.
- Camberlin, P., N. Martiny, N. Philippon, and Y. Richard (2007), Determinants of the interannual relationships between remote sensed photosynthetic activity and rainfall in tropical Africa, *Remote Sens. Environ.*, *106*, 199–216.
- Campos, G. E. P., et al. (2013), Ecosystem resilience despite large-scale altered hydroclimatic conditions, *Nature*, *494*, 349–352.
- Cayan, D. R., S. A. Kammerdiener, M. D. Dettinger, J. M. Caprio, and D. H. Peterson (2001), Changes in the onset of spring in the western United States, *Bull. Am. Meteorol. Soc.*, *82*(3), 399–415.
- Chapin, F. S., J. McFarland, A. D. McGuire, E. S. Euskirchen, R. W. Ruess, and K. Kielland (2009), The changing global carbon cycle: Linking plant–soil carbon dynamics to global consequences, *J. Ecol.*, *97*, 840–850.
- Clark, D. A., S. Brown, D. W. Kicklighter, J. Q. Chambers, J. R. Thomlinson, and J. Ni (2001), Measuring net primary production in forests: Concepts and field methods, *Ecol. Appl.*, *11*(2), 356–370.
- Coblentz, D. D., and K. H. Riitters (2004), Topographic controls on the regional-scale biodiversity of the south-western U.S.A., *J. Biogeogr.*, *31*, 1125–1138.
- Commission for Environmental Cooperation (1997), Ecological regions of North America. CEC, 71 pp.
- Cook, B. I., and R. Seager (2013), The response of the North American monsoon to increased greenhouse gas forcing, *J. Geophys. Res. Atmos.*, *118*, 1690–1699, doi:10.1002/jgrd.50111.
- Dai, A., P. J. Lamb, K. E. Trenberth, M. Hulme, P. D. Jones, and P. Xie (2004), The recent Sahel drought is real, *Int. J. Climatol.*, *24*, 1323–1331.
- Dominguez, F., P. Kumar, and E. R. Vivoni (2008), Precipitation recycling variability and ecoclimatological stability—A study using NARR data. Part II: North American monsoon region, *J. Clim.*, *21*(20), 5187–5203.
- Donohue, R. J., M. L. Roderick, T. R. McVicar, and G. D. Farquhar (2013), Impact of CO<sub>2</sub> fertilization on maximum foliage cover across the globe's warm, arid environments, *Geophys. Res. Lett.*, *40*, 3031–3035, doi:10.1002/grl.50563.
- Douglas, M. W., R. A. Maddox, K. Howard, and S. Reyes (1993), The Mexican monsoon, *J. Clim.*, *6*, 1665–1677.
- Eisfelder, C., C. Kuenzer, and S. Dech (2012), Derivation of biomass information for semi-arid areas using remote-sensing data, *Int. J. Remote Sens.*, *33*(9), 2937–2984.
- Fang, J., S. Piao, Z. Tang, C. Peng, and W. Ji (2001), Interannual variability in net primary production and precipitation, *Science*, *293*(5536), 1723.
- Fang, J., S. Piao, L. Zhou, J. He, F. Wei, R. B. Myneni, C. J. Tucker, and K. Tan (2005), Precipitation patterns alter growth of temperate vegetation, *Geophys. Res. Lett.*, *32*, L21411, doi:10.1029/2005GL024231.
- Fensholt, R., and S. R. Proud (2012), Evaluation of Earth observation based global long term vegetation trends—Comparing GIMMS and MODIS global NDVI time series, *Remote Sens. Environ.*, *119*, 131–147.
- Fensholt, R., et al. (2012), Greenness in semi-arid areas across the globe 1981–2007—An Earth Observing Satellite based analysis of trends and drivers, *Remote Sens. Environ.*, *121*, 144–158.
- Field, C. B., F. S. Chapin, P. A. Matson, and H. A. Mooney (1992), Responses of terrestrial ecosystems to the changing atmosphere—A resource-based approach, *Annu. Rev. Ecol. Evol. Syst.*, *23*, 201–235.
- Forzieri, G., F. Castelli, and E. R. Vivoni (2011), Vegetation dynamics within the North American monsoon region, *J. Clim.*, *24*, 1763–1783.
- Forzieri, G., E. R. Vivoni, and L. Feyen (2013), Ecosystem biophysical memory in the southwestern North American climate system, *Environ. Res. Lett.*, *8*, 044016, doi:10.1088/1748-9326/8/4/044016.
- Gobron, N., B. Pinty, and M. Verstraete (1998), Theoretical limits to the estimation of the leaf area index on the basis of visible and near-infrared remote sensing data, *IEEE Trans. Geosci. Remote Sens.*, *35*, 1438–1445.
- Gochis, A. J., L. Brito-Castillo, and W. J. Shuttleworth (2006), Hydroclimatology of the North American Monsoon region in northwest Mexico, *J. Hydrol.*, *316*, 53–70.
- Gochis, D. J., C. J. Watts, J. Garatuza-Payan, and J. C. Rodriguez (2007), Spatial and temporal patterns of precipitation intensity as observed by the NAME event rain gauge network from 2002 to 2004, *J. Clim.*, *20*, 1734–1750.
- Goward, S. N., and S. D. Prince (1995), Transient effects of climate on vegetation dynamics: Satellite observations, *J. Biogeogr.*, *22*, 549–563.
- Hartmann, D. L., et al. (2013), Observations: Atmosphere and Surface, in *Climate Change 2013: The Physical Science Basis*, Contribution of Working Group I to the Fifth Assessment Report of the Intergovernmental Panel on Climate Change, edited by T. F. Stocker et al., Cambridge Univ. Press, Cambridge, U. K., and New York.
- Higgins, R. W., J. E. Janowiak, and Y. Yao (1996), A gridded hourly precipitation data base for the United States (1963–1993). NCEP/Climate Prediction Center ATLAS 1, 47.
- Higgins, R. W., Y. Yao, and L. Wang (1997), Influence of the North American Monsoon System on the U.S. summer precipitation regime, *J. Clim.*, *10*, 2600–2622.
- Houghton, R. A. (2003), Revised estimates of the annual net flux of carbon to the atmosphere from changes in land use and land management 1850–2000, *Tellus, Ser. B*, *55*(2), 378–390, doi:10.1034/j.1600-0889.2003.01450.x.
- Huete, A. R., R. D. Jackson, and D. F. Post (1985), Spectral response of a plant canopy with different soil backgrounds, *Remote Sens. Environ.*, *17*, 37–53.
- Huete, A., K. Didan, T. Miura, E. P. Rodriguez, X. Gao, and L. G. Ferreira (2002), Overview of the radiometric and biophysical performance of the MODIS vegetation indices, *Remote Sens. Environ.*, *83*, 195–213.
- Hulshof, C. M., C. Violle, M. J. Spasojevic, B. McGill, E. Damschen, S. Harrison, and B. J. Enquist (2013), Intra-specific and inter-specific variation in specific leaf area reveal the importance of abiotic and biotic drivers of species diversity across elevation and latitude, *J. Veg. Sci.*, *24*, 921–931.
- Huxman, T. E., et al. (2004), Convergence across biomes to a common rain-use efficiency, *Nature*, *429*, 651–654.
- Ivits, E., S. Horion, R. Fensholt, and M. Cherlet (2013), Drought footprint on European ecosystems between 1999 and 2010 assessed by remotely sensed vegetation phenology and productivity, *Global Change Biol.*, *20*(2), 581–593.

- Jobbàgy, E. G., O. E. Sala, and J. M. Paruelo (2002), Patterns and controls of primary production in the Patagonian steppe: A remote sensing approach, *Ecology*, 83(2), 307–319.
- Keenan, T. F., et al. (2012), Terrestrial biosphere model performance for inter-annual variability of land-atmosphere CO<sub>2</sub> exchange, *Global Change Biol.*, 18, 1971–1987.
- Keenan, T. F., D. Y. Hollinger, G. Bohrer, D. Dragoni, J. W. Munger, H. P. Schmid, and A. D. Richardson (2013), Increase in forest water-use efficiency as atmospheric carbon dioxide concentrations rise, *Nature*, 499, 324–327.
- Kirtman, B., et al. (2013), Near-term climate change: Projections and predictability, in *Climate Change 2013: The Physical Science Basis*, Contribution of Working Group I to the Fifth Assessment Report of the Intergovernmental Panel on Climate Change, edited by T. F. Stocker, Cambridge Univ. Press, Cambridge, U. K., and New York.
- Knapp, A. K., and M. D. Smith (2001), Variation among biomes in temporal dynamics of aboveground primary production, *Science*, 291(5503), 481–484.
- Knohl, A., and D. D. Baldocchi (2008), Effects of diffuse radiation on canopy gas exchange processes in a forest ecosystem, *J. Geophys. Res.*, 113, G02023, doi:10.1029/2007JG000663.
- Lauenroth, W. K., I. C. Burke, and J. M. Paruelo (2000), Patterns of production and precipitation-use efficiency of winter wheat and native grasslands in the central Great Plains of the United States, *Ecosystems*, 3, 344–351.
- Le Houérou, H. N. (1984), Rain use efficiency: A unifying concept in arid-land ecology, *J. Arid. Environ.*, 7, 213–247.
- Leakey, A. D. B., E. Ainsworth, C. J. Bernacchi, A. Rogers, S. P. Long, and D. R. Ort (2009), Elevated CO<sub>2</sub> effects on plant carbon, nitrogen, and water relations: Six important lessons from FACE, *J. Exp. Bot.*, 60, 2859–76.
- Maloney, E. D., et al. (2014), North American climate in CMIP5 experiments: Part III: Assessment of twenty-first-century projections, *J. Clim.*, 27, 2230–2270.
- Mearns, L. O., et al. (2013), Climate change projections of the North American Regional Climate Change Assessment Program (NARCCAP), *Clim. Change*, 120(4), 965–975.
- Méndez-Barroso, L. A., and E. R. Vivoni (2010), Observed shifts in land surface conditions during the North American monsoon: Implications for a vegetation-rainfall feedback mechanism, *J. Arid. Environ.*, 74(5), 549–555.
- Méndez-Barroso, L. A., E. R. Vivoni, C. J. Watts, and J. C. Rodríguez (2009), Seasonal and interannual relation between precipitation, surface soil moisture and vegetation dynamics in the North American monsoon region, *J. Hydrol.*, 377, 59–70.
- Migliavacca, M., O. Sonnentag, T. F. Keenan, A. Cescatti, J. O'Keefe, and A. D. Richardson (2012), On the uncertainty of phenological responses to climate change, and implications for a terrestrial biosphere model, *Biogeosciences*, 9, 2063–2083.
- Mohamed, M. A. A., I. S. Babiker, Z. M. Chen, K. Ikeda, K. Ohta, and K. Kato (2004), The role of climate variability in the inter-annual variation of terrestrial net primary production (NPP), *Sci. Total Environ.*, 332, 123–137.
- Nemani, R. R., C. D. Keeling, H. Hashimoto, W. M. Jolly, S. C. Piper, C. J. Tucker, R. B. Myneni, and S. W. Running (2003), Climate-driven increases in global terrestrial net primary production from 1982 to 1999, *Science*, 300, 1560–1563.
- Nicholson, S. E., C. J. Tucker, and M. B. Ba (1998), Desertification, drought and surface vegetation: An example from the West African Sahel, *Bull. Am. Meteorol. Soc.*, 79, 815–829.
- Norby, R. J., and D. R. Zak (2011), Ecological lessons from Free-Air CO<sub>2</sub> enrichment (FACE) experiments, *Annu. Rev. Ecol. Evol. Syst.*, 42, 181–203.
- Notaro, M., A. Mauss, and J. W. Williams (2012), Projected vegetation changes for the American Southwest: Combined dynamic modeling and bioclimatic envelope approach, *Ecol. Appl.*, 22, 1365–1388.
- Noy-Meir, I. (1973), Desert ecosystems: Environment and producers, *Annu. Rev. Ecol. Evol. Syst.*, 4, 23–51.
- O'Connor, T. G., L. M. Haines, and H. A. Snyman (2001), Influence of precipitation and species composition on phytomass of a semi-arid African grassland, *J. Ecol.*, 89, 850–860.
- Ogle, K., and J. F. Reynolds (2004), Plant responses to precipitation in desert ecosystems: Integrating functional types, pulses, thresholds, and delays, *Oecologia*, 141(2), 282–294.
- Olson, R. J., J. M. O. Scurlock, S. D. Prince, D. L. Zheng, and K. R. Johnson (Eds) (2013), NPP multi-biome: NPP and driver data for Ecosystem Model-Data Intercomparison, R2. data set. Available on-line <http://daac.ornl.gov> from Oak Ridge National Laboratory Distributed Active Archive Center, Oak Ridge, Tennessee, doi:10.3334/ORNLDAAAC/615.
- Paruelo, J. M., and W. K. Lauenroth (1998), Interannual variability of NDVI and its relationship to climate for North American shrublands and grasslands, *J. Biogeogr.*, 25, 721–733.
- Paruelo, J. M., W. K. Lauenroth, I. C. Burke, and O. E. Sala (1999), Grassland precipitation-use efficiency varies across a resource gradient, *Ecosystems*, 2, 64–68.
- Pinzon, J., M. E. Brown, and C. J. Tucker (2005), Satellite time series correction of orbital drift artifacts using empirical mode decomposition, in *Hilbert-Huang Transform: Introduction and Applications*, edited by N. Huang, pp. 167–186, World Scientific, Singapore.
- Prince, S. D., E. Brown de Colson, and L. L. Kravitz (1998), Evidence from rain-use efficiency does not indicate extensive Sahelian desertification, *Global Change Biol.*, 4, 359–374.
- Prince, S. D., K. J. Wessels, C. J. Tucker, and S. E. Nicholson (2008), Desertification in the Sahel: A reinterpretation of a reinterpretation, *Global Change Biol.*, 13, 1308–1313.
- Quillet, A., C. Peng, and M. Garneau (2010), Toward dynamic global vegetation models for simulating vegetation–climate interactions and feedbacks: Recent developments, limitations, and future challenges, *Environ. Rev.*, 18, 333–353.
- Reed, B. C., J. F. Brown, D. VanderZee, T. R. Loveland, J. W. Merchant, and D. O. Ohlen (1994), Measuring phenological variability from satellite imagery, *J. Veg. Sci.*, 5, 703–714.
- Reynolds, J. F., P. R. Kemp, K. Ogle, and R. J. Fernandez (2004), Modifying the “pulse-reserve” paradigm for deserts of North America: Precipitation pulses, soil water and plant responses, *Oecologia*, 141(2), 194–210.
- Richardson, A. D., R. S. Anderson, and M. A. Arain (2012), Terrestrial biosphere models need better representation of vegetation phenology: Results from the North American Carbon Program Site Synthesis, *Global Change Biol.*, 18, 566–584.
- Rodríguez-Iturbe, I. (2000), Ecohydrology: A hydrologic perspective of climate-soil-vegetation dynamics, *Water Resour. Res.*, 36(1), 3–9, doi:10.1029/1999WR900210.
- Rodríguez-Iturbe, I., A. Porporato, F. Laio, and L. Ridolfi (2001), Intensive and extensive use of soil moisture: Plant strategies to cope with stochastic water availability, *Geophys. Res. Lett.*, 28(23), 4495–4497, doi:10.1029/2001GL012905.
- Running, S. W., R. R. Nemani, F. A. Heinsch, M. Chao, M. Reeve, and H. Hashimoto (2004), A continuous satellite-derived measure of global terrestrial primary production, *Bioscience*, 54(6), 547–560.
- Salinas-Zavala, C. A., A. V. Douglas, and H. F. Diaz (2002), Interannual variability of NDVI in northwest Mexico: Associated climatic mechanisms and ecological implications, *Remote Sens. Environ.*, 82(2–3), 417–430.

- Samanta, A., M. H. Costa, E. L. Nunes, S. A. Vieira, L. Xu, and R. B. Myneni (2011), Comment on "Drought-induced reduction in global terrestrial net primary production from 2000 through 2009", *Science*, 333, 1093.
- Saurer, M., et al. (2014), Spatial variability and temporal trends in water-use efficiency of European forests, *Global Change Biol.*, doi:10.1111/gcb.12717.
- Schwinning, S., and O. E. Sala (2004), Hierarchy of responses to resource pulses in arid and semi-arid ecosystems, *Oecologia*, 141, 211–220.
- Seager, R., et al. (2007), Model projections of an imminent transition to a more arid climate in southwestern North America, *Science*, 316, 1181.
- Sellers, P. C. (1985), Canopy reflectance, photosynthesis and transpiration, *Int. J. Remote Sens.*, 6, 1335–1372.
- Sheppard, P. R., A. C. Comrie, G. D. Packin, K. Angersbach, and M. K. Hughes (2002), The climate of the U.S. southwest, *Clim. Res.*, 21, 219–238.
- Siebert, S., V. Henrich, K. Frenken, and J. Burke (2013), *Global Map of Irrigation Areas Version 5*, Rheinische Friedrich-Wilhelms-University, Bonn, Germany/Food and Agriculture Organization of the United Nations, Rome, Italy.
- Swetnam, T. W., and J. L. Betancourt (1998), Mesoscale disturbance and ecological response to decadal climatic variability in the American Southwest, *J. Clim.*, 11, 3128–3147.
- Tarhule, A., and P. J. Lamb (2003), Climate research and seasonal forecasting for West Africans: Perceptions, dissemination, and use?, *Bull. Am. Meteorol. Soc.*, 84, 1741–1759.
- Thomas, S. C. (2011), Genetic vs. phenotypic responses of trees to altitude, *Tree Physiol.*, 31, 1161–1163.
- Tucker, C. J., J. E. Pinzon, and M. E. Brown (2004), Global inventory modeling and mapping studies. Global Land Cover Facility, University of Maryland, College Park, Rep. NA94apr15b.n11-Vlg, 2.0.
- Tucker, C. J., J. E. Pinzon, M. E. Brown, D. Slayback, E. W. Pak, R. Mahoney, E. Vermote, and N. Saleous (2005), An extended AVHRR 8-km NDVI data set compatible with MODIS and SPOT vegetation NDVI data, *Int. J. Remote Sens.*, 26, 4485–4498.
- Varnamkhasti, A. S., D. G. Milchunas, W. K. Lauenroth, and H. Goetz (1995), Production and rain use efficiency in short-grass steppe: Grazing history, defoliation and water resource, *J. Veg. Sci.*, 6, 787–796.
- Verón, S. R., M. Oesterheld, and J. M. Paruelo (2005), Production as a function of resource availability: Slopes and efficiencies are different, *J. Veg. Sci.*, 16, 351–354.
- Vivoni, E. R. (2012), Diagnosing seasonal vegetation impacts on evapotranspiration and its partitioning at the catchment scale during SMEX04-NAME, *J. Hydrometeorol.*, 13, 1631–1638.
- Vivoni, E. R., H. A. Gutiérrez-Jurado, C. A. Aragón, L. A. Méndez-Barroso, A. J. Rinehart, and R. L. Wyckoff (2007), Variation of hydrometeorological conditions along a topographic transect in northwestern Mexico during the North American monsoon, *J. Clim.*, 20(9), 1792–1809.
- Vivoni, E. R., H. A. Moreno, G. Mascaro, J. C. Rodríguez, C. J. Watts, J. Garatuza-Payán, and R. L. Scott (2008), Observed relation between evapotranspiration and soil moisture in the North American Monsoon Region, *Geophys. Res. Lett.*, 35, L22403, doi:10.1029/2008GL036001.
- Webb, W. L., W. K. Lauenroth, S. R. Szarek, and R. S. Kinerson (1986), Primary production and abiotic controls in forests, grasslands, and desert ecosystems of the United States, *Ecology*, 64, 134–151.
- Weltzin, J. F., et al. (2003), Assessing the response of terrestrial ecosystems to potential changes in precipitation, *BioScience*, 53, 941–952.
- White, M. A., P. E. Thornton, and S. W. Running (1997), A continental phenology model for monitoring vegetation responses to interannual climatic variability, *Global Biogeochem. Cycles*, 11, 217–234, doi:10.1029/97GB00330.
- Williams, A. P., et al. (2012), Temperature as potential driver of regional forest drought stress and tree mortality, *Nat. Clim. Change*, 3, 292–297.
- Yang, Y., J. Fang, W. Ma, and W. Wang (2008), Relationship between variability in aboveground net primary production and precipitation in global grasslands, *Geophys. Res. Lett.*, 35, L23710, doi:10.1029/2008GL035408.
- Yang, Y., F. Fang, P. A. Fay, J. E. Bell, and C. Ji (2010), Rain use efficiency across a precipitation gradient on the Tibetan Plateau, *Geophys. Res. Lett.*, 37, L15702, doi:10.1029/2010GL043920.
- Zhang, X., M. Goldberg, D. Tarpley, M. A. Friedl, J. Morissette, F. Kogan, and Y. Yu (2010), Drought-induced vegetation stress in southwestern North America, *Environ. Res. Lett.*, 5, 024008.
- Zhao, M., and S. W. Running (2010), Drought-induced reduction in global terrestrial net primary production from 2000 through 2009, *Science*, 329(5994), 940–943.
- Zhao, M., F. A. Heinsch, R. R. Nemani, and S. W. Running (2005), Improvements of the MODIS terrestrial gross and net primary production global data set, *Remote Sens. Environ.*, 95, 164–176.